ty in maintaining adequate voltage control of the large, highly infolded oocyte membrane with a two-microelectrode voltage clamp, and the changes in the time course of Na^+ channel inactivation that we have observed could have been obscured by the inappropriately slow inactivation of the Na^+ channels expressed in *Xenopus* oocytes (*5*).

The physiological significance of modulation of Na^+ channel activity in brain neurons by PKC is unknown. Types II and IIA Na^+ channels are preferentially localized in axons, whereas types I and III Na^+ channels are preferentially localized on neuronal cell bodies in vivo (*21*). Reduction and prolongation of Na^+ currents mediated by type II and IIA Na^+ channels in axons may alter the threshold for initiation of a conducted action potential and the frequency of action potential generation, and similar effects on Na^+ channels in nerve terminals may be expected to alter neurotransmitter release. Reduction of Na^+ currents by activation of PKC may also protect neurons against episodes of hyperexcitability. Further studies of the modulation of Na^+ channel function by PKC will be necessary to critically assess these possible physiological effects.

REFERENCES AND NOTES

1. L. Kaczmarek, *Trends Neurosci.* **10**, 30 (1987); M. S. Shearman, K. Sekiguchi, Y. Nishizuka, *Pharmacol. Rev.* **41**, 211 (1989); R. L. Huganir and P. Greengard, *Neuron* **5**, 555 (1990).
2. E. Sigel and R. Baur, *Proc. Natl. Acad. Sci. U.S.A.* **85**, 6192 (1988).
3. M. R. Costa and W. A. Catterall, *Cell. Mol. Neurobiol.* **4**, 291 (1984).
4. M. Noda *et al.*, *Nature* **320**, 188 (1986); T. Kayano, M. Noda, V. Flockerzi, H. Takahashi, S. Numa, *FEBS Lett.* **228**, 187 (1988).
5. V. J. Auld *et al.*, *Neuron* **1**, 449 (1988).
6. V. J. Auld *et al.*, *Proc. Natl. Acad. Sci. U.S.A.* **87**, 323 (1990).
7. A. L. Goldin *et al.*, *ibid.* **83**, 7503 (1986); M. Noda *et al.*, *Nature* **322**, 826 (1986); H. Suzuki *et al.*, *FEBS Lett.* **228**, 195 (1988).
8. T. Scheuer *et al.*, *Science* **247**, 854 (1990).
9. Primary rat brain cell cultures were prepared from day 20 embryos essentially as described [P. Vassilev, T. Scheuer, W. A. Catterall, *Proc. Natl. Acad. Sci. U.S.A.* **86**, 8147 (1989)]. Bipolar and pyramidal shaped cells were studied 2 to 6 days after plating.
10. J. W. Schmidt and W. A. Catterall, *J. Biol. Chem.* **262**, 13713 (1987).
11. O. P. Hamill, A. Marty, E. Neher, B. Sakmann, F. J. Sigworth, *Pfluegers Arch.* **391**, 85 (1981).
12. Patch-clamp experiments (*11*) were performed with the Axopatch 1C voltage clamp. The 500-megohm headstage resistor was used unless otherwise noted. Currents were digitally sampled at 40 kHz. Linear leakage and capacitance have been corrected by subtraction of null traces with no channel activity or scaled pulses recorded in voltage ranges where channel activity was absent. Current traces used for leakage subtraction were sometimes fit with a series of exponentials, and the resulting fit trace was used for subtraction to avoid addition of noise to the records. Solutions for generating outward currents in rat brain cells contained 140 mM NaCl, 20 mM CsCl, 5 mM Hepes, pH 7.4 in the recording pipette and 115 mM choline chloride, 20 mM tetraethylammonium chloride, 10 mM NaCl, 5 mM KCl, 1.5 mM $CaCl_2$, 1 mM $MgCl_2$, 5 mM glucose, 5 mM Hepes, pH 7.4 in the bath. Measurement of outward Na^+ currents does not make the voltage homogeneous throughout the length of the neurites of cultured rat brain neurons but does improve the quality of the recorded Na^+ currents by preventing regenerative activity. Solutions for cell-attached and excised patch recording from CNaIIA-1 cells contained 150 mM KCl, 10 mM NaCl, 1.5 mM $CaCl_2$, 2 mM $MgCl_2$, 1 mM EGTA, 5 mM Hepes, KOH to pH 7.4 in the bath and 150 mM NaCl, 5 mM KCl, 1.5 mM $CaCl_2$, 1 mM $MgCl_2$, pH 7.4 in the recording pipette. All recordings were performed at room temperature (approximately 22°C). Peptide inhibitors of protein kinase A [cAMP-dependent protein kinase inhibitor (PKI) 5-24, Peninsula Labs] and of PKC were dissolved in 150 mM KCl before microinjection. PMA, DOG, and OAG were dissolved in dimethyl sulfoxide at concentrations of 10, 8.33, and 8.33 mM, respectively, and stored at −20°C until use. The pseudosubstrate site inhibitor peptide of PKC was a gift of K. Meier and E. G. Krebs. PMA was obtained from Calbiochem. All other chemicals were obtained from Sigma.
13. CNaIIA-1 cells are Chinese hamster ovary cells (CHO-K1, American Type Culture) that have been stably transfected by calcium phosphate precipitation [D. Chen and H. Okayama, *Mol. Cell. Biol.* **7**, 2745 (1987)] with the plasmid pZem228/SP6 containing the coding sequence for the rat brain type IIA Na^+ channel α subunit under control of the mammalian metallothionein promoter. pZem228/SP6 is a variant of Zem228 [C. Clegg *et al.*, *J. Biol. Chem.* **262**, 13111 (1987)] and contains the *neo* gene, conferring G418 resistance. Transfected cells were maintained in RPMI (Gibco), 10% fetal calf serum (Hyclone), and G418 (200 μg/ml) (Gibco). The type IIA Na^+ channel sequence contains the natural leucine at position 860, which confers a normal voltage dependence of activation and inactivation (*5, 6*). Transfected cells express large voltage-dependent Na^+ currents (4 to 25 nA). CNaIIA-1 cells have also been referred to as C81-11 cells, our original laboratory designation (*14*).
14. T. Scheuer, J. W. West, L. Maechler, W. A. Catterall, *Biophys. J.* **59**, 262a (1991).
15. P. Hockberger, M. Toselli, D. Swandulla, H. D. Lux, *Nature* **338**, 340 (1989).
16. C. House and B. E. Kemp, *Science* **238**, 1726 (1987). We microinjected inhibitor peptides into individual cells by orally applying positive pressure to the back of an injection pipette. Successful cytoplasmic injections were monitored visually as a slight cytoplasmic swelling that relaxed when the pipette was withdrawn.
17. S. G. Rane, M. P. Walsh, J. R. McDonald, K. Dunlap, *Neuron* **3**, 239 (1989).
18. H.-C. Cheng *et al.*, *J. Biol. Chem.* **261**, 989 (1986); H.-C. Cheng, S. M. Van Patten, A. J. Smith, D. A. Walsh, *Biochem. J.* **231**, 655 (1985).
19. PKC was purified as described [J. R. Woodgett and T. Hunter, *J. Biol. Chem.* **262**, 4836 (1987)]. The purified enzyme was activated with 1 μM diolein (1,2 dioleoyl-sn-glycerol) (Sigma) and 1 μM phosphatidylserine. Diolein (10 μg/ml) and phosphatidylserine (0.5 mg/ml) in a 10 mM tris stock solution were stored at −20°C.
20. N. Dascal and I. Lotan, *Neuron* **6**, 165 (1991).
21. R. E. Westenbroek, D. K. Merrick, W. A. Catterall, *ibid.* **3**, 695 (1989); unpublished results.

22. Supported by NIH research grants NS15751 and NS25704 to W.A.C. We thank B. Murphy, M. Ahlijanian, and Y. Lai for providing protein kinase C; K. Meier and E. G. Krebs for supplying the pseudosubstrate site inhibitor peptide of PKC; G. Eaholtz for preparation of embryonic rat brain cell cultures; C. Warner for maintenance of CNaIIA-1 cell cultures; R. Walsh for secretarial assistance; and B. Hille for valuable discussions and critical comments on the manuscript.

13 May 1991; accepted 27 June 1991

Establishment of the Mesoderm-Neuroectoderm Boundary in the *Drosophila* Embryo

DAVID KOSMAN, Y. TONY IP, MICHAEL LEVINE, KAVITA ARORA

A gradient of the maternal morphogen *dorsal* establishes asymmetric patterns of gene expression along the dorsal-ventral axis of early embryos and activates the regulatory genes *twist* and *snail*, which are responsible for the differentiation of the ventral mesoderm. Expression of *snail* is restricted to the presumptive mesoderm, and the sharp lateral limits of this expression help to define the mesoderm-neuroectoderm boundary by repressing the expression of regulatory genes that are responsible for the differentiation of the neuroectoderm. The *snail* gene encodes a zinc finger protein, and neuroectodermal genes that are normally restricted to ventral-lateral regions of early embryos are expressed throughout ventral regions of *snail*$^-$ mutants. The formation of the sharp *snail* border involves dosage-sensitive interactions between *dorsal* and *twist*, which encode regulatory proteins that are related to the mammalian transcription factors NF-kB and MyoD, respectively.

A POLYCLONAL ANTIBODY TO *SNAIL* (*sna*) (*1*) was prepared against a *sna* protein made in *Escherichia coli* (*2*). The bacterial protein contains 287 amino acid residues and lacks 102 NH_2-terminal residues present in the native *sna* protein. The resulting antibody (*3*) was used to monitor *sna* expression during embryogenesis (Fig. 1). The protein was detected by the onset of cleavage cycle 14, and, by the middle of cycle 14, its distribution appeared to coincide with the presumptive mesoderm (Fig. 1A). The borders of the *sna* pattern were sharp in lateral regions (arrow) and at the boundary between the presumptive mesoderm and posterior midgut invagination (PMG) (arrowhead). Expression persisted in the differentiating mesoderm throughout the formation of the ventral furrow (Fig. 1B) and the initial phases of germ-band elongation (Fig. 1C). After germ band elon-

Biology Department, Center for Molecular Genetics, University of California, San Diego, La Jolla, CA 92093.

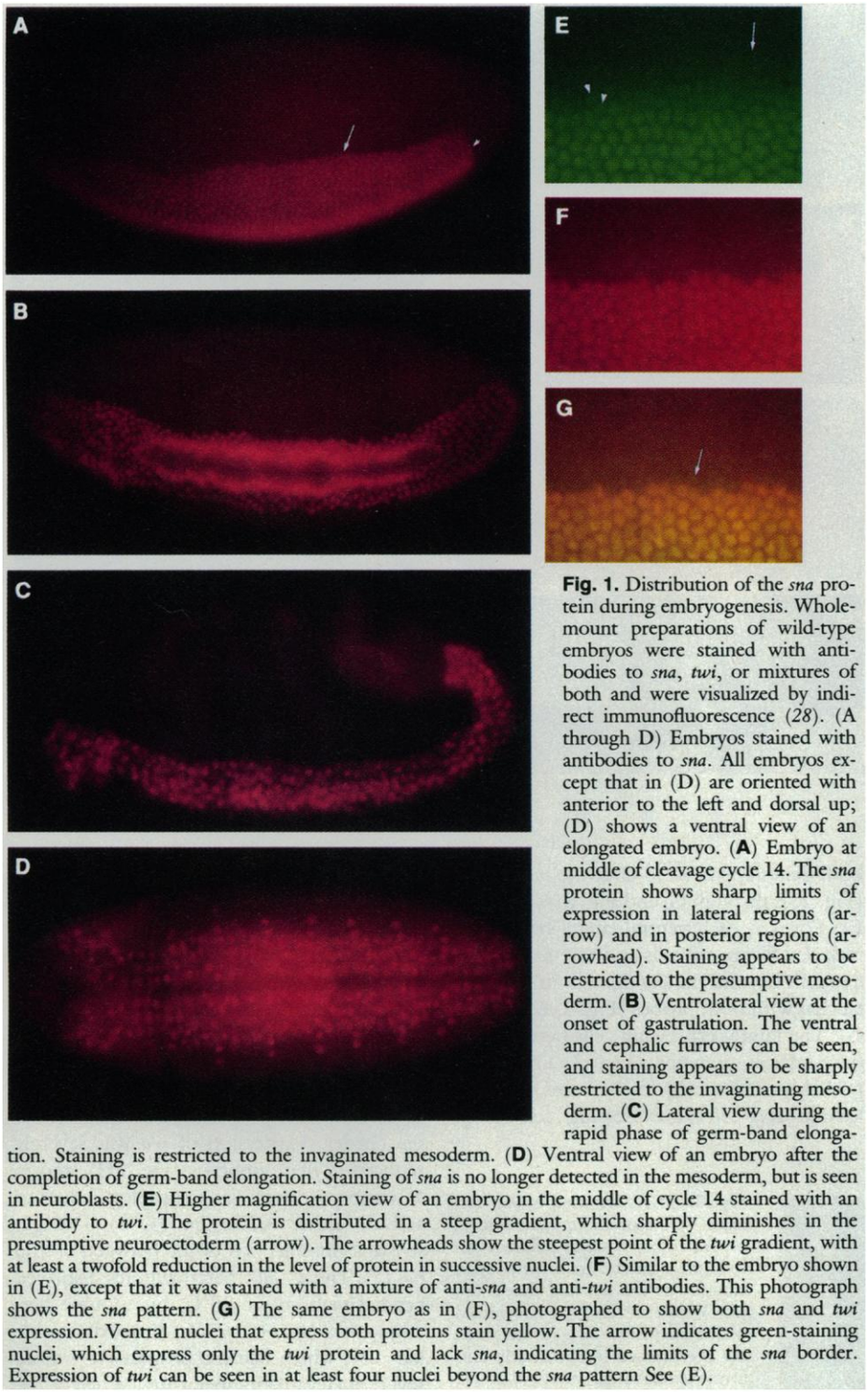

Fig. 1. Distribution of the *sna* protein during embryogenesis. Whole-mount preparations of wild-type embryos were stained with antibodies to *sna*, *twi*, or mixtures of both and were visualized by indirect immunofluorescence (*28*). (A through D) Embryos stained with antibodies to *sna*. All embryos except that in (D) are oriented with anterior to the left and dorsal up; (D) shows a ventral view of an elongated embryo. (**A**) Embryo at middle of cleavage cycle 14. The *sna* protein shows sharp limits of expression in lateral regions (arrow) and in posterior regions (arrowhead). Staining appears to be restricted to the presumptive mesoderm. (**B**) Ventrolateral view at the onset of gastrulation. The ventral and cephalic furrows can be seen, and staining appears to be sharply restricted to the invaginating mesoderm. (**C**) Lateral view during the rapid phase of germ-band elongation. Staining is restricted to the invaginated mesoderm. (**D**) Ventral view of an embryo after the completion of germ-band elongation. Staining of *sna* is no longer detected in the mesoderm, but is seen in neuroblasts. (**E**) Higher magnification view of an embryo in the middle of cycle 14 stained with an antibody to *twi*. The protein is distributed in a steep gradient, which sharply diminishes in the presumptive neuroectoderm (arrow). The arrowheads show the steepest point of the *twi* gradient, with at least a twofold reduction in the level of protein in successive nuclei. (**F**) Similar to the embryo shown in (E), except that it was stained with a mixture of anti-*sna* and anti-*twi* antibodies. This photograph shows the *sna* pattern. (**G**) The same embryo as in (F), photographed to show both *sna* and *twi* expression. Ventral nuclei that express both proteins stain yellow. The arrow indicates green-staining nuclei, which express only the *twi* protein and lack *sna*, indicating the limits of the *sna* border. Expression of *twi* can be seen in at least four nuclei beyond the *sna* pattern See (E).

gation, expression was lost in the ventral mesoderm but reappeared later in all neuroblasts as they segregated from the neuroectoderm (Fig. 1D). In contrast to an earlier report (*1*), our antibody does not detect *sna* protein in the cytoplasm of differentiating neurons.

The *sna* expression pattern is similar, but not identical, to the *twist* (*twi*) pattern (*4–6*). Whereas *sna* RNAs and proteins are only transiently expressed in the presumptive mesoderm, *twi* expression persists well after the time when *sna* products are no longer detected and continues during the initial periods of muscle differentiation (*5*). Sustained expression of *twi* suggests that it might be important in mesoderm differentiation. In contrast, the transience of the *sna* pattern suggests involvement only in the initiation of the mesodermal pathway. This distinction is not evident in the mutant phenotypes of sna^- or twi^- embryos, which display similar losses of the mesoderm and its derivatives (*6, 7*).

Double-staining studies indicated that the *twi* and *sna* expression patterns overlap but do not coincide. Expression of *twi* was not restricted to the presumptive mesoderm but was seen to be graded and extended into the ventral neuroectoderm (Fig. 1E, arrow). In contrast, the *sna* pattern showed a sharp on-off border in the same lateral regions (Fig. 1F) and appeared to coincide with the presumptive mesoderm. Double-labeling experiments revealed that *sna* expression ends abruptly at the steepest point of the *twi* gradient, where there is at least a twofold reduction in the level of protein (Fig. 1G).

To determine the roles of *twi* and *sna* in the differentiation of the neuroectoderm, we examined the expression of *lethal of scute* (*T3*) and *rhomboid* (*rho*) in wild-type and mutant embryos. *T3* is contained within the achaete-scute gene complex (AS-C) and encodes a helix-loop-helix regulatory protein that is important for the differentiation of neuroblasts within the neuroectoderm (*8–10*). *T3* transcripts were initially detected in ventral-lateral regions of precellular embryos, and during gastrulation these transcripts were distributed in a series of seven pair-rule stripes that quickly evolved into 14 hemistripes (Fig. 2A). In sna^- mutant embryos, the *T3* pattern was expanded so that expression extended throughout ventral regions that normally form the mesoderm. Thus, *sna* appeared to restrict *T3* expression to ventral-lateral regions of wild-type embryos.

In contrast, *twi* appeared to exert a weak positive effect on *T3* expression. There was a delay of at least 30 min in the time when *T3* transcripts could first be detected in twi^- embryos, as compared with wild-type embryos (*11*). By the onset of gastrulation, there was a partial derepression of the *T3* pattern in ventral regions of twi^- embryos, but this was less dramatic than that seen in *sna* mutants (Fig. 2, B and C). It is possible that this weak derepression is indirect and mediated by *sna* because there is a marked reduction in the amount of *sna* transcripts in twi^- embryos (Fig. 2, D and H). These results suggest that one way in which *twi* initiates the mesodermal pathway is by enhancing the expression of *sna*, which in turn blocks the activities of genes that direct alternative pathways of development.

Further support for this view stems from studies with the *spitz* group gene *rho*, which encodes a putative transmembrane protein that participates in the differentiation of the mesectoderm (see below) and a subset of ventral epidermal cells from the neuroectoderm (*12, 13*). As with *T3*, the initial *rho* pattern appeared to be delimited by the *sna* border. When *rho* transcripts were first de-

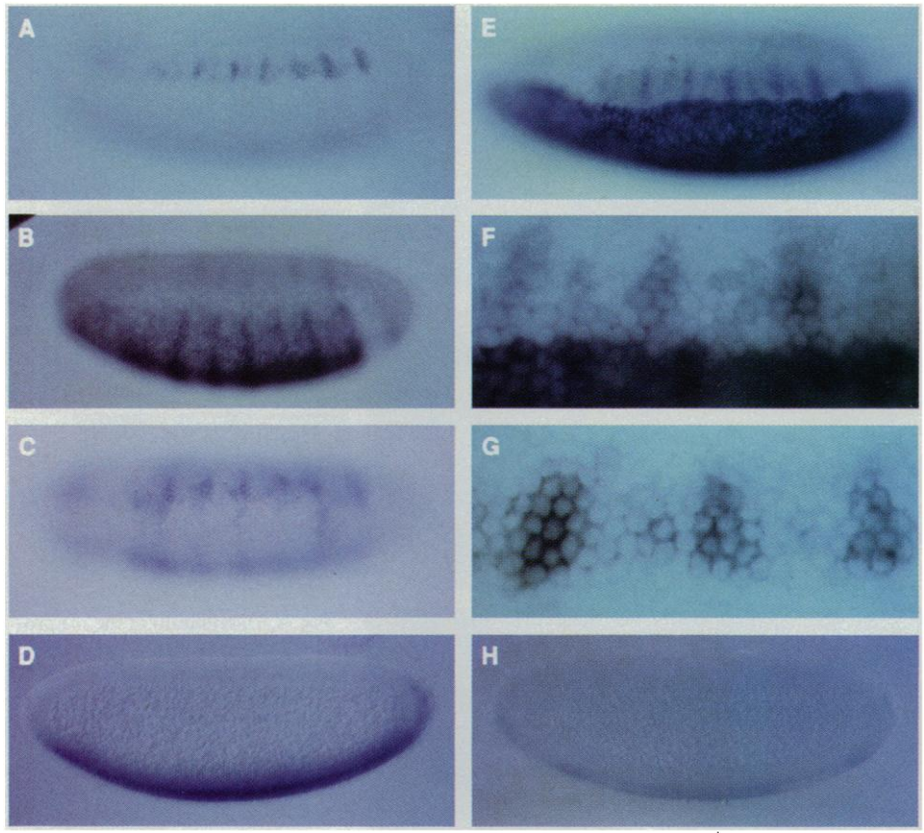

Fig. 2. *T3* and *sna* RNAs in wild-type and mutant embryos. Whole-mount preparations of embryos were hybridized with *sna*, *T3*, or mixtures of both DNA probes, and their corresponding RNAs were visualized histochemically (*30*). All embryos are at similar stages, spanning from the middle of cleavage cycle 14 through cellularization and are oriented with anterior to the left. (**A**) Wild-type embryo hybridized with a *T3* probe. This embryo is undergoing the transition from a 7- to 14-stripe pattern. These hemistripes are sharply restricted to ventrolateral regions running along both sides of the embryo (only one side can be seen in this photograph). (**B**) A sna^- embryo that is oriented somewhat more ventrally than those shown in (A) and (C) (*31*). *T3* expression extends throughout ventral regions that normally give rise to the mesoderm. (**C**) A twi^- embryo showing slight ventral derepression of the *T3* pattern (*31*). Expression is significantly weaker than in wild-type embryos at comparable stages. (**D**) Wild-type embryo showing the *sna* RNA pattern. (**E**) Wild-type embryo simultaneously hybridized with *T3* and *sna* probes. The *T3* hemistripes appear to abut the *sna* border. (**F**) Higher magnification of an embryo similar to the one shown in (E). (**G**) Higher magnification of a wild-type embryo hybridized with the *T3* probe alone. Each hemistripe includes about five to six cells, which appear to extend from the *sna* border in the doubly labeled embryo shown in (F). (**H**) A twi^- embryo hybridized with a *sna* probe. There are ventral gaps in the pattern. Expression is substantially reduced as compared to that in the wild-type embryo shown in (D). The embryos shown in (E) and (H) were stained in the same experiment.

tected in a wild-type embryo, they were distributed in two broad, ventral-lateral bands that extended along the length of the embryo (Fig. 3A). In sna^- embryos, these bands expanded to include ventral regions that normally form the mesoderm (Fig. 3B). There was a delay and partial expansion of *rho* expression in twi^- embryos (*11*).

The *sna* gene might exert a direct repressive effect on *T3* and *rho* expression because both genes appeared to abut the *sna* border (Fig. 2, E through G, and Fig. 3, C through E). For *T3*, each ventral-lateral hemistripe included five to six cells and extended about five cells beyond the *sna* domain in embryos labeled with both probes (Fig. 2, E through G). The faintly expressing cells between the *rho* and *sna* domains (Fig. 3, C and E) probably correspond to the most ventrally located row of *rho*-expressing cells (Fig. 3D). Additional experiments were done with the regulatory gene *single minded* (*sim*), which encodes a helix-loop-helix protein that plays a key role in the differentiation of the mesectoderm (*14, 15*). The *sim* gene also abuts the *sna* border and is expressed in sna^- embryos (*11, 16, 17*). Thus, *T3*, *rho*, and *sim* all appear to obey the *sna* border.

Both *dorsal* (*dl*) and *twi* gene activities are required for the proper establishment of the *sna* border. Expression of *sna* was severely reduced in twi^- embryos (Fig. 2H), and in dl^- embryos there was a complete failure to activate either *twi* or *sna* (*5, 6*). Dosage-sensitive interactions occur between *dl* and *twi* (7). The dl^-/dl^+ heterozygotes displayed normal viability at 25°C, but double heterozygotes ($dl^-/+$,$twi^-/+$) showed variable lethality, which became progressively more severe at elevated temperatures. When $dl^-/+$ mothers were mated with $twi^-/+$ males at 25°C, only 20% of the expected number of $twi^-/+$ heterozygotes survived, and the lethal embryos showed defects in mesoderm formation similar to those observed in *twi* mutants (7). On the basis of analysis of *twi* and *sna* expression in the double heterozygotes, it appears that the lethality is due to a marked reduction in the limits of both *twi* and *sna* expression (Fig. 4). The most consistent defects were narrower ventral-lateral limits of expression and gaps in the pattern

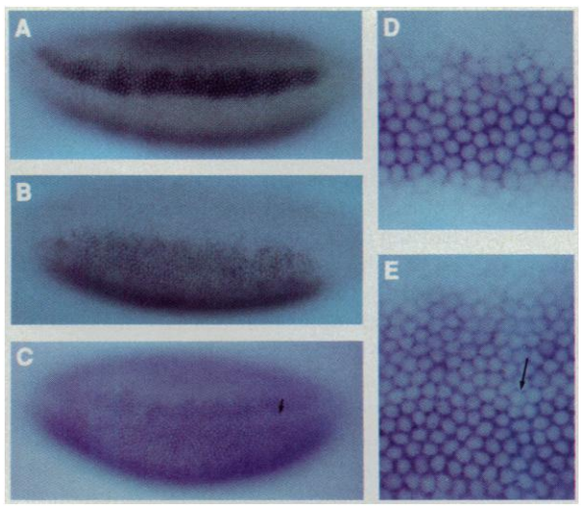

Fig. 3. RNAs encoded by *rho* and *sna* in wild-type and mutant embryos. All embryos are at cellular blastoderm stages and are oriented with anterior to the left and dorsal up. (**A**) Wild-type embryo hybridized with a *rho* probe (*32*). At this time, *rho* is expressed in two nearly uniform ventrolateral bands that extend along the length of the embryo. Expression includes most of the presumptive ventral neuroectoderm (*12*). (**B**) A sna^- embryo hybridized with a *rho* probe. There is a dramatic increase of expression in the ventral cells that normally form mesoderm. (**C**) Wild-type embryo hybridized with a mixture of *sna* and *rho* probes. (**D**) Higher magnification of a wild-type embryo hybridized with a *rho* probe. The reduced amounts of staining in the most ventral expressing cells could account for the apparent gap between the *sna* and *rho* patterns indicated by the arrow in (C) and (E). (**E**) Higher magnification of the embryo shown in (C).

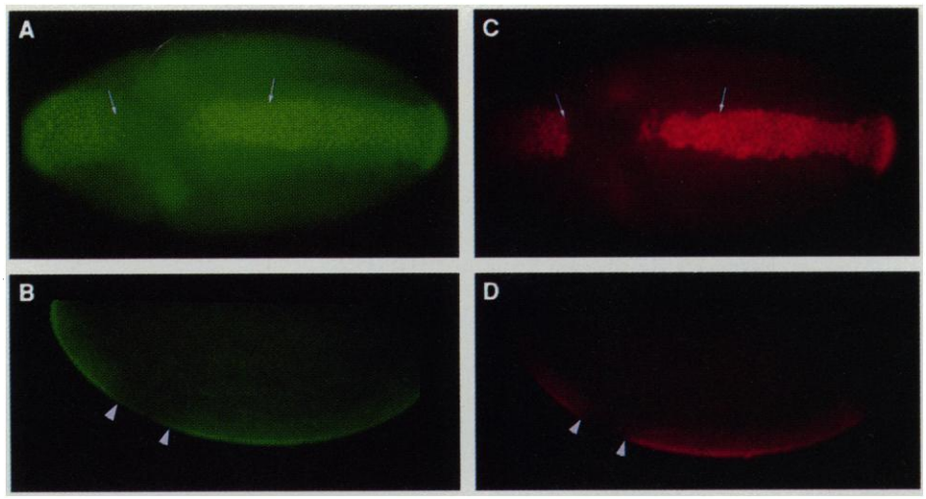

Fig. 4. Expression of *twi* and *sna* in dl^{-}/+,twi^{-}/+ double heterozygotes. Embryos were collected from a mating of dl^{-}/+ females and twi^{-}/+ males and grown at 25°C (*31*). The embryos were stained with mixtures of antibodies to *twi* and *sna*, and are oriented with anterior to the left. (**A**) Ventral view of a gastrulating embryo showing *twi* expression in green. The lateral limits of expression are reduced and there is a significant reduction near the cephalic furrow (arrows). There is no indication of a ventral furrow, which is seen in comparable wild-type embryos. (**B**) Lateral view of a precellular embryo showing *twi* staining. There is reduced expression near the region of the presumptive cephalic furrow (arrowheads). (**C**) The same embryo as in (A), showing *sna* expression in red. As seen for *twi*, the lateral limits are severely reduced, and there is a loss of expression near the cephalic furrow. (**D**) The same embryo [as in (B)] showing *sna* expression. The arrowheads indicate a region where *sna* expression is lost, which corresponds to the site of reduced *twi* staining.

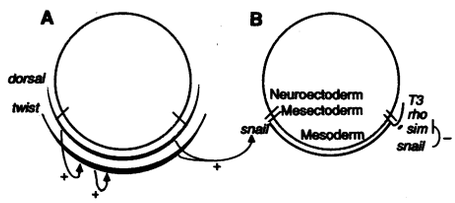

Fig. 5. Summary of the role of *dl* in defining the mesoderm-neuroectoderm boundary. The two circles represent cross sections of a precellular (**A**) and a cellular blastoderm-stage embryo (**B**), which contains a total of 72 cells in its circumference. The gradient of nuclear *dl* protein extends from the ventral surface to the lateral midline. A dose-dependent threshold response to *dl* initiates the expression of *twi*, and then *dl* and *twi* act in concert to specify a somewhat steeper gradient of *twi* than is observed for *dl* (*19*). The *twi* protein pattern ends about five cells beyond the limits of the presumptive mesoderm (indicated by the solid diagonal lines in the diagram). The *dl* and *twi* gradients specify sharp borders of *sna* expression, which in turn represses regulatory genes active in the presumptive mesectoderm and neuroectoderm, including *T3*, *rho*, and *sim*.

in anterior regions near the cephalic furrow (Fig. 4, A and C). The embryo shown in Fig. 4, A and C, is undergoing gastrulation, but there is a failure of ventral furrow formation. Normally, the *sna* pattern includes a band ~18 cells wide along the ventral midline (see Fig. 1B), but, in this mutant embryo, the *sna* domain is only ~10 cells wide (Fig. 4C). Double heterozygotes that contained more than ten *sna*-expressing cells usually displayed ventral furrows, whereas embryos expressing fewer than eight or nine cells failed to invaginate. This situation is reminiscent of gastrulation in sea urchins, where ingression of a minimal threshold number of cells is required to provide sufficient local force for the invagination of the vegetal plate (*18*).

Despite the disruptions in the *twi* and *sna* patterns seen in dl^{-}/+,twi^{-}/+ heterozygotes, they displayed the same relative limits of expression observed in wild-type embryos. For example, the *twi* pattern was graded, with progressively less protein expressed beyond the sharp *sna* border (Fig. 4, A and C). As in the wild-type embryo, a twofold reduction in the level of *twi* protein correlated with a sharp on-off border of *sna* expression. Moreover, there was a disproportionate reduction in *twi* expression in the presumptive cephalic furrow (Fig. 4B). Staining of *twi* was reduced in this region, and there was a dramatic loss of *sna* expression (Fig. 4, B and D). These results suggest that *dl* and *twi* may act in concert to establish the full lateral limits of *twi* expression and the sharp *sna* borders (Fig. 5). According to this model, *dl* activates *twi*, and the initially low amounts of *twi* protein in lateral regions are enhanced through a positive autofeedback mechanism (*19*). The catastrophic narrowing of the *twi* pattern observed in *dl*,*twi* double heterozygotes might be caused by reduced levels of *twi* protein that are below the critical threshold required for autoregulation.

We have presented evidence that *sna* establishes a sharp boundary between the presumptive mesoderm and neuroectoderm by repressing the expression of regulatory genes (*T3* and *rho*) responsible for the differentiation of neuroectodermal derivatives, including neuroblasts, glial cells, and ventral epidermis (Fig. 5). The expression patterns of several neurogenic genes, such as *Delta* (*20*), suggest that they might also obey the *sna* border.

The lateral limits of *sna* expression may be determined by cooperative interactions between the shallow *dl* gradient and the steeper *twi* gradient (Fig. 5). The *sna* gene encodes a zinc finger protein (*6*) that might function as a direct transcriptional repressor. There is evidence that repression by *sna* could be relatively direct: the slight derepression of *T3* and *rho* observed in twi^{-} embryos correlates with reduced expression of *sna*. Moreover, there are ventral expansions of the *T3* and *rho* patterns in dl^{-}/+,twi^{-}/+ heterozygotes, which correlate with the severity in the reduction of *sna* expression (*11*). However, the coexpression of *T3* and *sna* in neuroblasts suggests that this repression might involve a second regulatory factor, such as *dl*, that is active only in early embryos.

Small amounts of *twi* protein in the presumptive neuroectoderm may define cell fate. This situation would be analogous to the functional redundancy provided by low amounts of the *bicoid* morphogen and the gap protein *hunchback* in regulating *Kruppel* expression in central regions of the embryo (*21*). Alternatively, this expression may be a fortuitous consequence of the way in which the *twi* promoter responds to the *dl* concentration gradient. The finding that *sim* expression is abolished and *T3* reduced in *twi*,*sna* double mutants (*11, 17*) supports the view that *twi* is important for the differentiation of the mesectoderm and neuroectoderm.

There are numerous examples of dosage-sensitive interactions between genes involved in a common developmental pathway, including sex determination and neurogenesis. The reduction in the lateral limits of *twi* and *sna* expression observed in dl^{-}/+,twi^{-}/+ double heterozygotes could be the result of two distinct transcription factors acting on a common target gene. The *dl* gene is a member of the *rel* family of DNA binding proteins (*22*), whereas *twi* contains a helix-loop-helix motif (*23*). Specific *dl* and *twi* binding sites may be present in essential control regions of the *twi* and *sna* promoters. The two proteins may interact to mediate cooperative binding to DNA or, alternatively, may activate transcription through synergistic contacts with the transcription complex (*24*).

We propose that *sna* allows *twi* to function as a mesodermal determinant by repressing the expression of *sim* (*16*), AS-C (*10*), E(spl) (*25*), and other regulatory genes responsible for the differentiation of the mesectoderm and neuroectoderm. In *sna* embryos, ventral cells that normally form mesoderm now express the wrong regulatory genes, and consequently follow an alternative fate.

Note added in proof: Similar results on the role of *sna* in mesoderm formation have been obtained (*25a*).

REFERENCES AND NOTES

1. J. L. Boulay, C. Dennefeld, A. Alberga, *Nature* **330**, 395 (1987); A. Alberga, J.-L. Boulay, E. Kempe, C. Dennefeld, M. Haenlin, *Development* **111**, 983 (1991).
2. A synthetic 36-nucleotide oligomer was synthesized that is complementary to a region of the *sna* protein coding sequence (*1*). The oligomer was used to screen a 4- to 8-hour cDNA plasmid library (*26*). Three hybridizing clones were purified and their restriction maps were found to correspond to the *sna* map (*1*). One of the clones was partially sequenced so that its identity as a *sna* cDNA could be confirmed. An 880–base pair (bp) Nde I restriction fragment from the cDNA, containing coding sequences from amino acid residues 103 to 390 was inserted into the unique Nde I site of the bacterial pAR3040 T7 expression plasmid. The *sna* peptide was overexpressed in the BL21 (DE3) strain (*27*).
3. Preparative quantities of the *sna* peptide were isolated from SDS-polyacrylamide gels and used for immunization of a guinea pig (Pocono Farms, PA). The serum was diluted 1:200 in phosphate-buffered saline, 1% bovine serum albumin, 0.5 M NaCl, 0.1% Tween-80, and was used to stain whole-mount preparations of formaldehyde-methanol–fixed embryos (*28*). The protein was visualized using a tetramethyl rhodamine isothiocyanate-conjugated antibody to guinea pig (Jackson Immunoresearch, Bethesda, MD) diluted in the same staining buffer. Staining of *twi* was done with a rabbit antibody provided by S. Roth *et al.* (*29*), and visualized with a fluorescein isothiocyanate–conjugated secondary antibody (Jackson Immunoresearch). Fluorescence microscopy was done with a Nikon Optiphot microscope, and photographs were taken with Kodak Kodachrome film (Asa 64).
4. B. Thisse *et al.*, *Genes Dev.* **1**, 709 (1987).
5. B. Thisse *et al.*, *EMBO J.* **7**, 2175 (1988).
6. M. Leptin and B. Grunewald, *Development* **110**, 73 (1990).
7. P. Simpson, *Genetics* **105**, 615 (1983).
8. R. Villares and C. V. Cabrera, *Cell* **50**, 415 (1987).
9. M. C. Alonso and C. V. Cabrera, *EMBO J.* **7**, 2588 (1988).
10. C. V. Cabrera, A. Martinez-Arias, M. Bate, *Cell* **50**, 425 (1987); S. Romani, S. Campuzano, J. Modolell, *EMBO J.* **6**, 2085 (1987).
11. D. Kosman and M. Levine, unpublished results.
12. E. Bier, L. Y. Jan, Y. N. Jan, *Genes Dev.* **4**, 190 (1990).
13. U. Mayer and C. Nusslein-Volhard, *ibid.* **2**, 1496 (1988).
14. S. Crews, J. Thomas, C. S. Goodman, *Cell* **52**, 143 (1988).
15. J. Thomas, S. Crews, C. S. Goodman, *ibid.*, p. 133.
16. J. R. Nambu *et al.*, *ibid.* **63**, 63 (1990).
17. C. Rushlow and K. Arora, *Seminars Cell Biol.* **1**, 137 (1990).
18. D. R. McClay and C. A. Ettensohn, *Annu. Rev. Cell Biol.* **3**, 319 (1987).
19. We have obtained evidence that *twi* exerts a positive effect on its own expression. The levels and the spatial limits of *twi* RNAs are markedly reduced in a protein null mutant (*twi* ID96).
20. M. Haenlin, B. Kramatscheck, J. A. Campos-Ortega, *Development* **110**, 905 (1990).
21. M. Hulskamp, C. Pfeifle, D. Tautz, *Nature* **346**, 577 (1990).
22. Y. T. Ip *et al.*, *Cell* **64**, 439 (1991).
23. C. Murre, P. McCaw, D. Baltimore, *ibid.* **56**, 777 (1989).
24. Y. Lin *et al*, *Nature* **345**, 359 (1990).
25. J. A. Campos-Ortega and E. Knust, *Eur. J. Biochem.* **190**, 1 (1990).
25a. M. Leptin, *Genes Dev.* **5**, 1568 (1991).
26. N. H. Brown and F. C. Kafatos, *J. Mol. Biol.* **203**, 425 (1988).
27. R. W. Studier and B. A. Moffatt, *ibid.* **189**, 113 (1986).
28. T. Mitchison and J. Sedat, *Dev. Biol.* **99**, 261 (1983).
29. S. Roth, D. Stein, C. Nusslein-Volhard, *Cell* **59**, 1189 (1989).
30. RNAs were localized by means of the whole-mount in situ hybridization method developed by D. Tautz and C. Pfeifle [*Chromosoma* **98**, 81 (1989)]; the *sna* probe that was used for hybridization corresponded to an 880-bp Nde I restriction fragment from the full-length cDNA, whereas the *T3* probe was a 1-kb genomic DNA fragment (provided by J. Modellel and M. Caudy).
31. The following mutant alleles were used in this study: *twist*, ID96 (*29*); *snail*, IIG05 (*6*); and *dorsal*, dl-8 (*29*).
32. The *rho* probe used for whole-mount hybridizations corresponded to a 2.5-kb Eco RI restriction fragment from a cDNA (provided by E. Bier).

33. We thank M. Caudy and J. Modolell for *T3* DNA, E. Bier for the *rho* DNA, N. Brown for the cDNA library, S. Roth for the *twi* antibody, R. Kraut for helpful discussions, S. Small for help with the photography, and C. Rushlow, R. Warrior, B. Harris, and E. Bier for critical readings of the manuscript. Supported in part by the American Chemical Society and by NIH grant GM 46638.

25 February 1991; accepted 30 May 1991

Technical Comment

Mathematical Analysis of a Model of the Mitotic Clock

In their mathematical model of the cyclin and maturation promotion factor (MPF) system, Norel and Agur (*1*) note that oscillations occurred if the degradation of cyclin had saturable kinetics but not if the reaction was first order with respect to cyclin. One might ask whether this saturability is mathematically necessary for oscillation, or whether the investigators just did not find the right parameters for the first-order case. In the same vein, one might ask whether the degradation of MPF must have saturable kinetics (as assumed) and whether the autocatalytic term for the formation of MPF must be of order greater than 1 with respect to MPF.

These questions can be answered by analyzing the effect of reaction order on stability, following Higgins (*2*). Let M and C denote the concentrations of active MPF and cyclin, respectively, and $\dot{M}$ and $\dot{C}$ the rates of change in these concentrations. For a closed trajectory around a single critical point [that is, a point (M,C) where $\dot{M} = \dot{C} = 0$], the Poincaré theorem requires

$$(\partial\dot{M}/\partial M)(\partial\dot{C}/\partial C) - (\partial\dot{M}/\partial C)(\partial\dot{C}/\partial M) > 0 \quad (1)$$

at the critical point. A sufficient condition for instability at the critical point is

$$\partial\dot{M}/\partial M + \partial\dot{C}/\partial C > 0 \quad (2)$$

These equations can be restated in terms of orders and rates of reaction at the critical point, the order of reaction with respect to X being defined as $(X/V)(\partial V/\partial X)$, where V is the reaction rate. So defined, reaction order may depend on concentration and must be evaluated at the critical point for our present purposes. The rates of change of M and C in the Norel and Agur model are the differences between rates of formation and rates of removal:

$$\dot{M} = F_M - R_M \text{ and } \dot{C} = F_C - R_C$$

Then, for example, $\partial\dot{M}/\partial M = \partial F_M/\partial M - \partial R_M/\partial M$. Let ϕ_{MX} and ρ_{MX} be the orders of reaction for F_M and R_M, respectively, with respect to X, for example,

$$\phi_{MM} = (M/F_M)(\partial F_M/\partial M)$$

Then, because $F_M = R_M$ and $F_C = R_C$ at the critical point,

$$\partial M/\partial M = (F_M/M)(\phi_{MM} - \rho_{MM})$$

and Eqs. 1 and 2 become

$$(\phi_{MM} - \rho_{MM})(\phi_{CC} - \rho_{CC}) - (\phi_{MC} - \rho_{MC})(\phi_{CM} - \rho_{CM}) > 0 \quad (3)$$

and

$$\frac{F_M}{M}(\phi_{MM} - \rho_{MM}) + \frac{F_C}{C}(\phi_{CC} - \rho_{CC}) > 0 \quad (4)$$

In the Norel and Agur model, $\rho_{MC} = \phi_{CM} = \phi_{CC} = 0$, and $\phi_{MC} = \rho_{CM} = 1$; so Eqs. 3 and 4 become

$$(\phi_{MM} - \rho_{MM})\rho_{CC} < 1 \quad (5)$$

and

$$(\phi_{MM} - \rho_{MM}) > \frac{MF_C}{F_M C}\rho_{CC} \quad (6)$$